Supporting Information

Ligand-coordinated Ir Single-atom Catalysts Stabilized on Oxide Supports for Ethylene Hydrogenation and Their Evolution under a Reductive Atmosphere

Linxiao Chen,[1,†] Iyad S. Ali,[1] George E. Sterbinsky,[2] Xuemei Zhou,[1,‡] Eman Wasim,[1] and Steven L. Tait[1,*]

[1] Dept. of Chemistry, Indiana University, Bloomington, Indiana 47405, USA

[2] Advanced Photon Source, Argonne National Laboratory, Lemont, Illinois 60439, USA

* E-mail: tait@indiana.edu, Tel: +1-812-855-1302

[†] Present address: Institute for Integrated Catalysis, Pacific Northwest National Laboratory, Richland, Washington 99352, USA

[‡] Present address: School of Chemical Engineering, Sichuan University, No. 24 South Section 1, Yihuan Road, Chengdu, 610065, P.R.C.

Table of Contents

Section 1. Supplemental XAS Data and Comments

Comments on EXAFS fittings

First-shell EXAFS fittings were performed using the Artemis software (version 0.9.26).[1] For all supported Ir SACs, two shells were considered: Ir−O/N and Ir−Cl. The former might include contributions from Ir binding with O/N from ligands and O from oxide supports. As shown in our previous works with Pt, M−O and M−N shells are too similar in EXAFS to be considered separately.[2, 3] For post-reaction samples, appropriate fittings can be achieved by including only these two shells (Figure 2a-c bottom, and Table S1). Including an Ir−C=C shell (from ethylene adsorption), did not improve fittings significantly. This is because π adsorption of ethylene on Ir single-atoms is not particularly strong and hence should be removed easily.

All fitting parameters are listed in Table S1 and Table S2. For each shell, ΔR and σ^2 were set as independent parameters. ΔE_o was assumed to be the same for both shells. S_0^2 was determined to have a value of 0.85 by fitting Na_2IrCl_6 and K_3IrCl_6 standards measured during the same beamline time, and it was fixed to this value for both shells. For all samples, keeping both N(Ir−O/N) and N(Ir−Cl) as independent parameters was feasible (7 total independent parameters), but this strategy generally yielded large standard deviations for fitting parameters. Therefore, we slightly modified the strategy. An initial fitting was performed with variable N for both paths. Then we fixed N(Ir−Cl) to 10 values around the initial fitting value and the XPS Cl : Ir ratio (the two numbers are always relatively consistent), to obtain the fitting with best quality (measured by reduced chi-square) and all parameters within ranges allowed by rules of physics (such as $\sigma^2 > 0$). This strategy reduces standard deviations significantly to an acceptable level, while yielding results similar to those found when keeping both N flexible. For all *ex situ*

samples (Figure 2a-c, Figure S1-3, and Table S1) and *in situ* samples (Figure 7d, and Table S2) up to t = 4.8 h, the above strategy and model are able to fit EXAFS data well.

We did notice that as H_2 treatment on Ir-PDO/MgO proceeds, EXAFS features become wider (**Figure S4**). There appears to be weak residual intensity around 2.3 Å in the Fourier transform magnitude of the k^2-weighted EXAFS spectrum starting from t = 4.8 h. We are confident that the residual is not consistent with Ir−Ir, Ir−H−Ir, or Ir−O−Ir scattering so it does not represent Ir aggregation of any form. One possibility is that during the H_2 treatment, the rearrangement of the Ir-oxide interface leads to formation of Ir−Mg or longer Ir−O bonds. Nevertheless, the position is too far for normal direct Ir−O bonds (~1.6 Å) and too close for Ir−Mg bonds calculated from Ir_2Mg alloy (2.6 Å). Attempts to fit the spectra with Ir−Mg did not yield improved results. While the origin of this observation remains to be explored, our fittings still match well with EXAFS data (**Figure S3b**, bottom). For completeness, we also present all EXAFS spectra (Fourier transform magnitude) without any fittings in **Figure S4**. These show that one can easily perceive the drop in first-shell scattering intensity even without fittings, which clearly supports our conclusion that Ir lose coordination with O/N and Cl during H_2 treatment beyond the uncertainties of EXAFS fittings (**Figure 7d**).

Table S1. The full list of EXAFS fitting parameters of metal-ligand Ir SACs.[1] Coordination numbers (CN) from these fittings are presented as **Table 2**, indicating total first-shell CN around 7 on all fresh SACs. The lack of Ir−Ir or Ir−O−Ir paths (no Ir aggregation) are shared characters for all fresh, post-reaction, and post-H_2 samples in this study, suggesting excellent stability of our Ir single-atoms.

		WL intensity	N(Ir−O/N)	R(Ir−O/N) / Å	σ^2(Ir−O/N) / 10^{-3}	N(Ir−Cl)[2]	R(Ir−Cl) / Å	σ^2(Ir−Cl) / 10^{-3}	ΔE_o / eV	k-range
Ir-PDO /CeO_2	Fresh	2.86	5 (1)	2.03 (0.02)	9 (4)	2.3	2.33 (0.01)	2 (1)	8 (2)	3~12
	Post-reaction	2.74	5.7 (0.7)	2.04 (0.01)	8 (2)	1.3	2.34 (0.01)	2 (1)	9 (1)	3~12
	Post-H_2	2.76	6 (3)	2.04 (0.05)	9 (8)	1.3	2.32 (0.05)	4 (7)	9 (4)	3~10
Ir-DPTZ /CeO_2	Fresh	2.77	4 (1)	2.03 (0.03)	7 (6)	3.3	2.35 (0.01)	1.4 (0.8)	8 (2)	3~13
	Post-reaction	2.65	4.7 (0.4)	2.05 (0.03)	10 (1)	2.2	2.35 (0.01)	1.1 (0.8)	9 (2)	3~12
Ir-PDO /MgO	Fresh	2.69	4.1 (0.9)	2.05 (0.02)	7 (4)	2.8	2.36 (0.01)	1.2 (0.6)	11 (1)	3~13.7
	Post-reaction	2.61	5.4 (0.9)	2.03 (0.02)	7 (3)	0.3	2.26 (0.08)	4 (8)	10 (2)	3~12
	Post-H_2[3]	2.15	0.9 (0.2)	2.05 (0.05)	1.0 (0.3)	1.1	2.39 (0.03)	1.0 (0.1)	16 (3)	3~10
Ir-DPTZ /MgO	Fresh	2.83	3.5 (0.4)	2.05 (0.01)	10 (1)	3.7	2.35 (0.01)	1.2 (0.5)	8.8 (0.6)	3~10.5

[1] For all fittings, S_o^2 was fixed to 0.85 based on fittings results of K_3IrCl_6 and Na_2IrCl_6.
[2] N(Ir−Cl) was manually varied to obtain the best reasonable fitting, so a standard deviation is not reported. Keeping both N(Ir−Cl) and N(Ir−O/N) as independent parameters yielded similar results but significantly larger standard deviations in all parameters.
[3] The maximum allowed free parameters is at least 8.4. All fittings in this and the next tables have 6 free parameters.

Table S2. The full list of EXAFS fitting parameters of Ir-PDO/MgO during the *in situ* experiment.[1] Raw EXAFS spectra in *R*-space (magnitude, without fittings) are shown as **Figure S4** below. Fitting results listed in this table were used to generate Figure 7d. Each EXAFS spectrum is an average of multiple scans, so it represents average structural information within this time span. The H_2-to-He and He-to-H_2 switch were made at t = 6.7 h and 11.8 h respectively.

	Time / h	N(Ir−O/N)	R(Ir−O/N) / Å	σ^2(Ir−O/N) / 10^{-3}	N(Ir−Cl)[2]	R(Ir−Cl) / Å	σ^2(Ir−Cl) / 10^{-3}	ΔE_o / eV	k-range
Fresh	0	3.8 (1.1)	2.03 (0.03)	7 (5)	3.0	2.36 (0.01)	1 (1)	10 (2)	3~12
H_2	0.7	3.5 (1.4)	2.06 (0.05)	6 (7)	2.2	2.37 (0.02)	4 (2)	10 (3)	3~11
	1.2	2.7 (0.6)	2.03 (0.02)	4 (3)	2.0	2.36 (0.01)	1 (1)	9 (1)	3~11
	2.5	1.9 (0.5)	2.03 (0.02)	3 (3)	1.6	2.36 (0.01)	1 (1)	9 (2)	3~11
	4.8	1.5 (0.5)	2.03 (0.03)	3 (5)	1.3	2.37 (0.02)	2 (2)	11 (2)	3~11
He	9.1	1.3 (0.5)	2.01 (0.03)	2 (5)	1.2	2.36 (0.02)	1 (1)	11 (2)	3~11
H_2	12.9	1.1 (0.5)	2.05 (0.04)	2 (7)	1.1	2.38 (0.03)	2 (2)	15 (3)	3~11
	17.0	0.9 (0.2)	2.04 (0.05)	1.0 (0.3)	1.1	2.39 (0.03)	1.0 (0.2)	15 (3)	3~10

[1] For all fittings, S_o^2 was fixed to 0.85 based on fittings results of K_3IrCl_6 and Na_2IrCl_6.
[2] N(Ir−Cl) was manually varied to obtain the best and reasonable fitting, and hence standard deviation is not applicable.

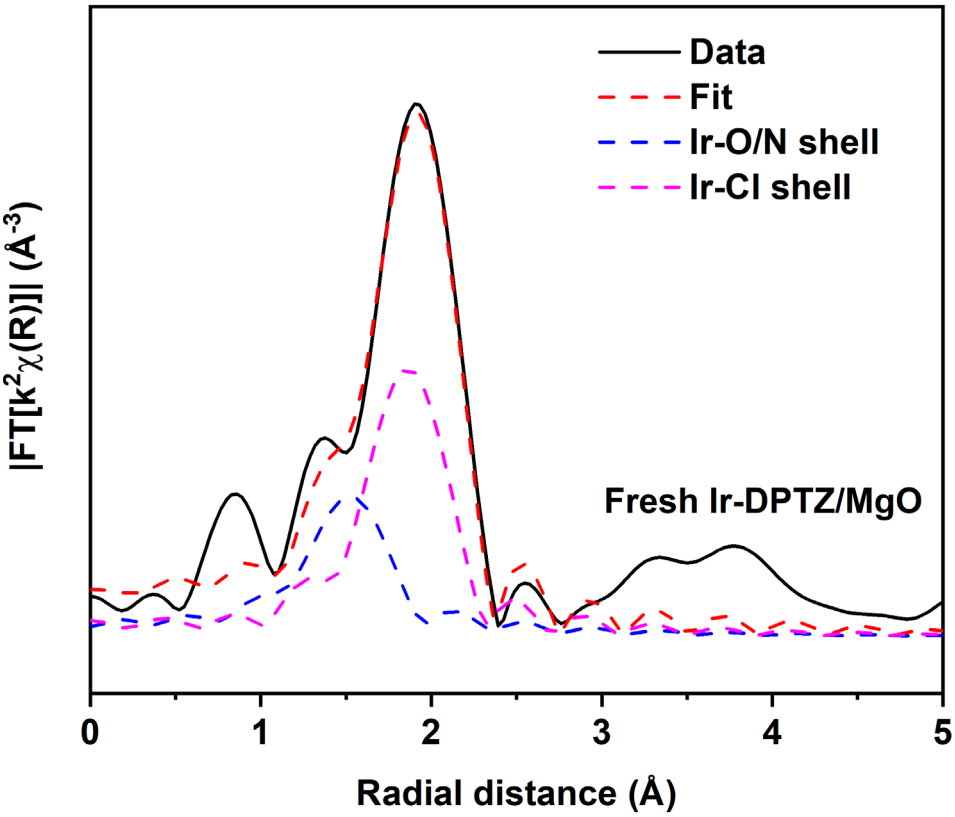

Figure S1. EXAFS of fresh Ir-DPTZ/MgO SAC in *R*-space (magnitude) with first-shell fittings.

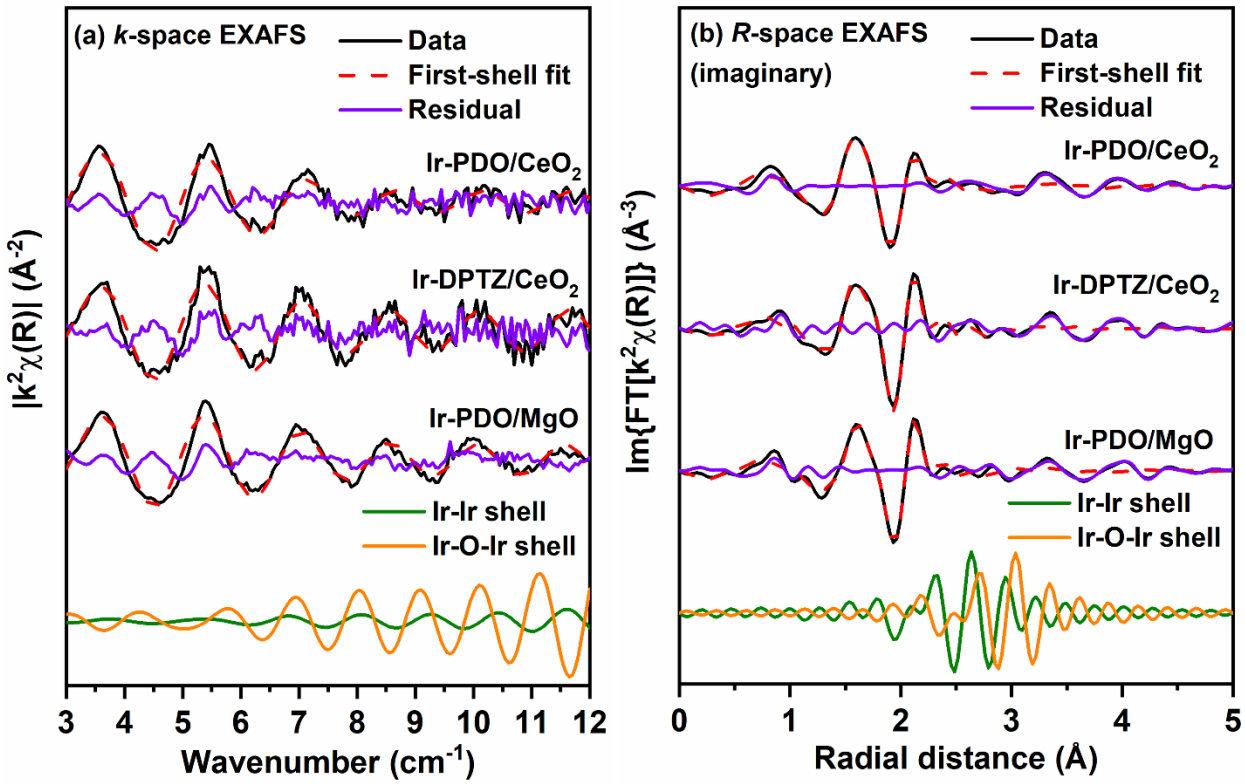

Figure S2. EXAFS of fresh Ir-PDO/CeO_2, Ir-DPTZ/CeO_2, and Ir-PDO/MgO SAC in (a) *k*-space and (b) *R*-space (imaginary component). In each graph, the first shell fitting is compared to the data and the residual values are plotted as the purple trace. The residuals from the first-shell fittings with Ir−O/N and Ir−Cl paths (R-space magnitude shown in **Figures 2a-2c**, top) do not resemble either Ir−Ir or Ir−O−Ir shells, further confirming that in all cases, Ir do not form detectable aggregates.

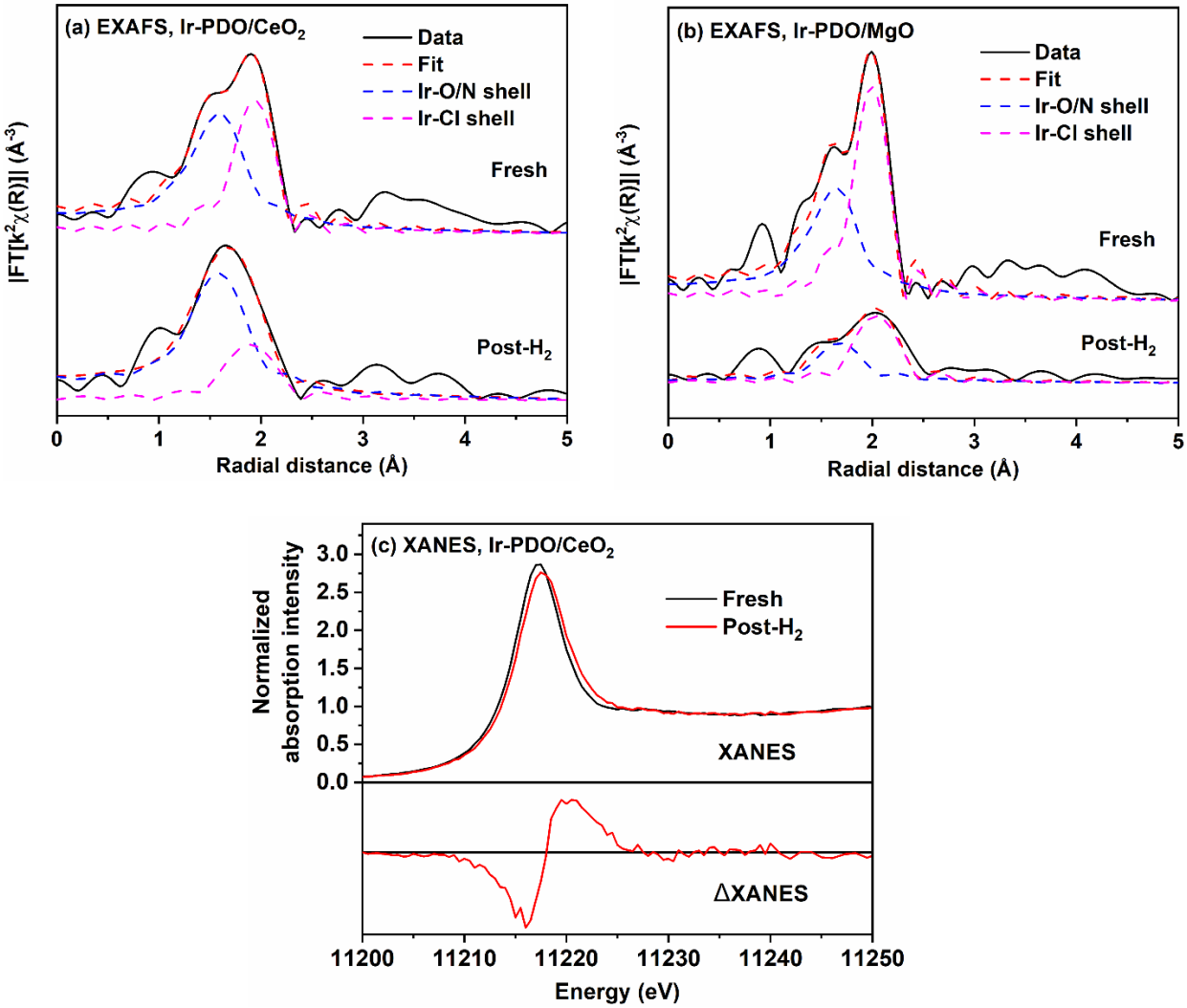

Figure S3. EXAFS of fresh and post-H_2 Ir-PDO SACs in *R*-space (magnitude) with first-shell fittings on (a) CeO_2 and (b) MgO. In both graphs, there is no contribution from Ir−Ir shells, suggesting that long-term (15 h for CeO_2 and 13 h for MgO) H_2 treatment at 100 °C does not lead to formation of reduced Ir clusters. In the bottom spectrum of **Figure S3b**, there is some residual intensity at ~2.3 Å, implying that the fitting model only including Ir−O/N and Ir−Cl shells may not be completely accurate. Nevertheless, the position of the residual is not consistent with Ir−Ir. It may arise from Ir−Mg scattering or a different type of Ir−O scattering formed during the H_2 treatment. (c) XANES and ΔXANES of fresh and post-H_2 Ir-PDO/CeO_2, showing the slight reduction of Ir (decrease in white line intensity and shift in edge energy) and the presence of a small amount of Ir−H (the secondary feature beyond the white line).

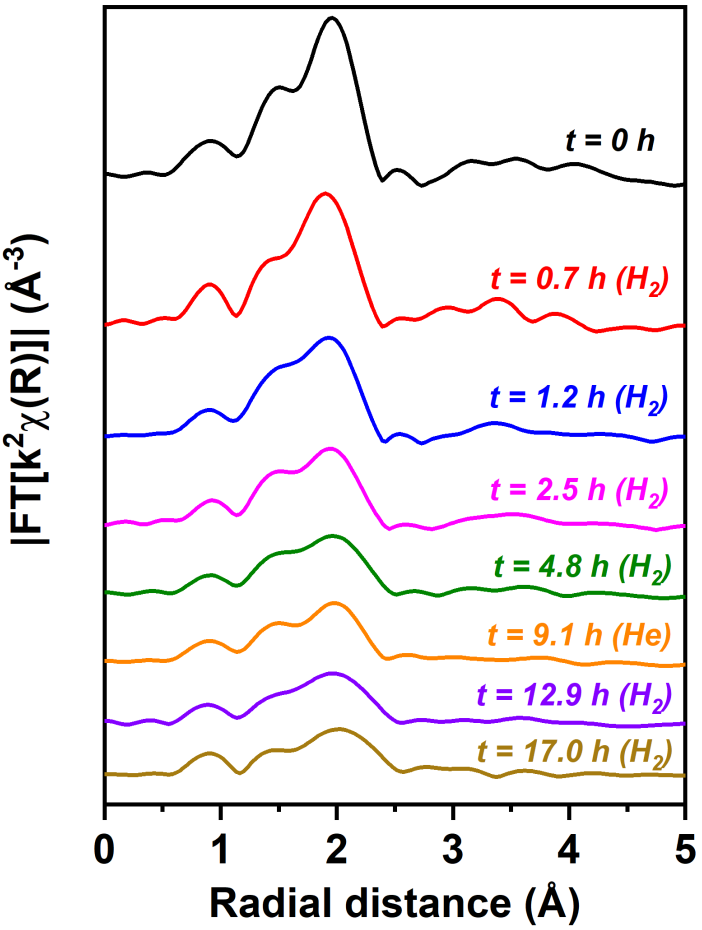

Figure S4. EXAFS of Ir-PDO/MgO during the *in situ* experiment in *R*-space (magnitude) without fittings. The overall decrease in scattering intensity between 1 and 3 Å is obvious in these raw data even without performing fittings, strongly suggesting the loss of Ir−O and Ir−Cl coordination in the first shell. First-shell fitting results of the spectra are presented in **Table S2** and **Figure 7d**.

Comments on formal oxidation states of Ir

We attempted to assign formal oxidation states of Ir according to the white line intensity or edge position in XANES. However, neither of these correlate well with Ir oxidation states for the standard Ir compounds that were measured (**Figure S5b-S5c**). Literature suggests that when antibonding orbitals of ligands interact strongly with the metal, white line intensity increases due to electron back donation.[4-6] This is exhibited by $Ir(CO)_2(AcAc)$ (**Figure S5b**), which is an Ir(I) compound with ligands offering strong Ir 5*d*-π* interactions and has much higher white line intensity than the other Ir(I) compound tested, $[Ir(COD)Cl]_2$. For this reason, all our fresh Ir SACs show higher white line intensity than Ir(IV) standard Na_2IrCl_6 (**Figure S5a**, **Table S2**) despite XPS showing lower Ir 4*f* binding energy than $IrCl_4$ (**Figure 3**). Therefore, comparing Ir oxidation states based on white line intensity should be done with caution. It is only proper when ligands around the metal are similar, or no ligands with strong metal-π* back donation are present.

Despite the fact that we are not confident assigning a specific formal oxidation state to Ir single-atoms, we are confident that Ir single-atoms exist in a non-metallic oxidized form because of the high white line intensity in XANES relative to that of Ir(0), binding energy in Ir 4*f* XPS, and CO adsorption peak position (**Figure 4**). Our previous studies on Pt SACs show that Pt is reduced from Pt(IV) in precursor to Pt(II) during the synthesis.[2, 3] In the case of Ir, binding energy of Ir $4f_{7/2}$ XPS peak of all Ir SACs is clearly lower than $IrCl_4$ precursor. Ir(II) has been rarely seen in the literature, and the CO vibration energy of Ir^{m+}−CO species is significantly higher than previous reports on supported Ir(I) complexes.[7] Consequently, we think Ir in these SACs are likely Ir(III), which is a common stable oxidation states among homogeneous Ir catalysts.

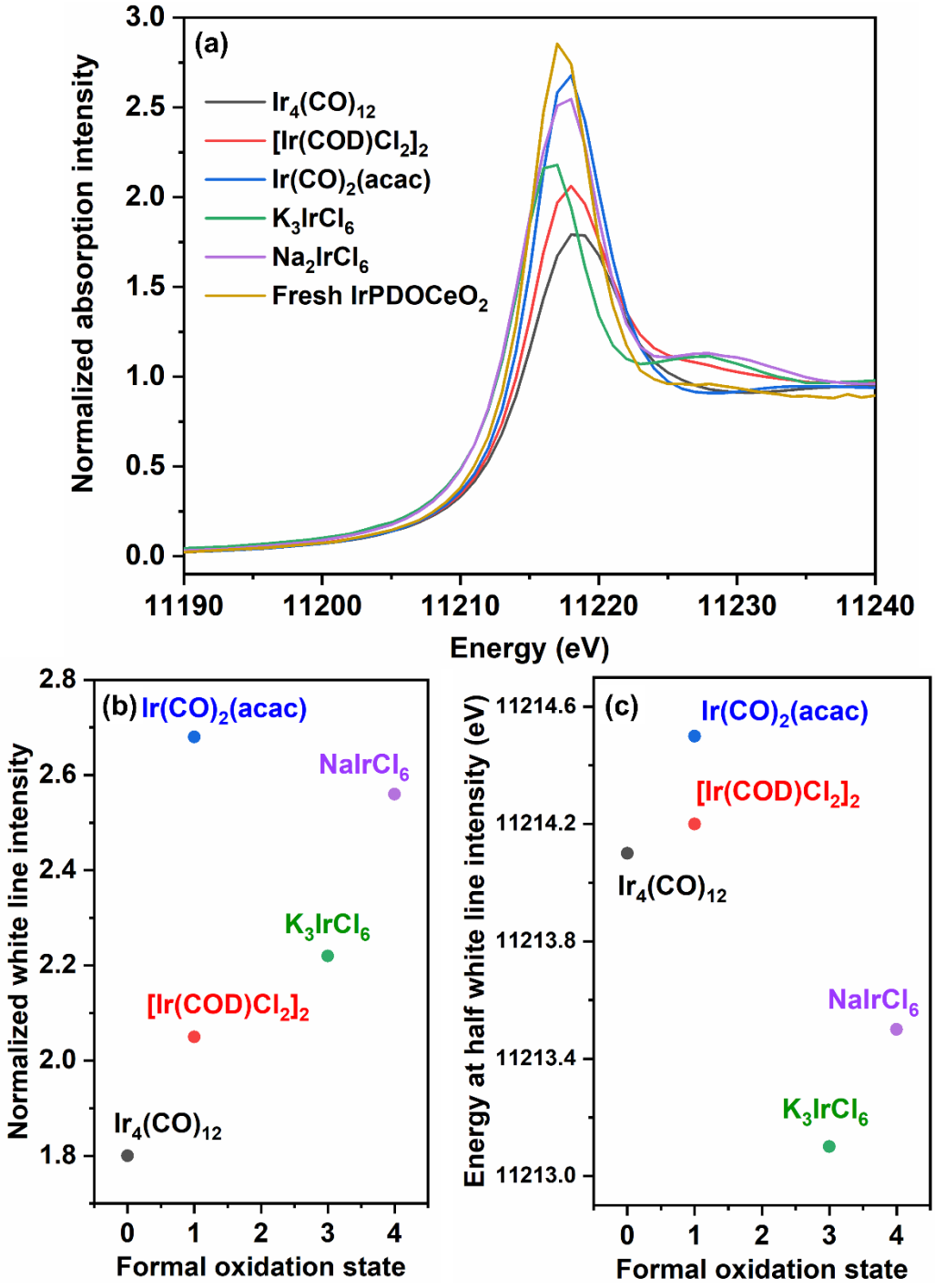

Figure S5. XANES results from various Ir standard compounds. (a) Actual XANES spectra from measurements. (b) Relationship between white line intensity and formal oxidation state of Ir. (c) Relationship between edge position (represented by the energy at half white line intensity) and formal oxidation state of Ir.

Section 2. Supplemental Characterization Results from Other Techniques

Table S3. Summary of XPS results on Ir-ligand SACs.

	Ir-PDO/CeO_2			Ir-DPTZ/CeO_2		Ir-PDO/MgO		
	Fresh	Post-reaction	Post-H_2	Fresh	Post-reaction	Fresh	Post-reaction	Post-H_2
Ligand : Ir	0.93	0.86	0.84	0.23	0.19	0.44	0.38	0.27
Cl : Ir	2.7	1.8	1.5	3.5	2.5	2.9	2.7	3.0
Ir 4*f* BE	62.2	62.2	61.8	62.3	62.2	62.3	61.9	62.0
Ir $4f_{7/2}$ FWHM	1.6	1.9	2.1	1.6	1.6	2.0	2.0	2.0

We note that each ligand has two binding pockets, and thus offers up to 4 O/N atoms to coordinate with Ir. Meanwhile, besides the ligand and Cl, Ir also bind with surface O from the oxide supports. Therefore, the relatively high ligand : Ir and Cl : Ir values from XPS imply a crowded Ir coordination sphere on fresh catalysts, consistent with N values from EXAFS fitting (Table 2).

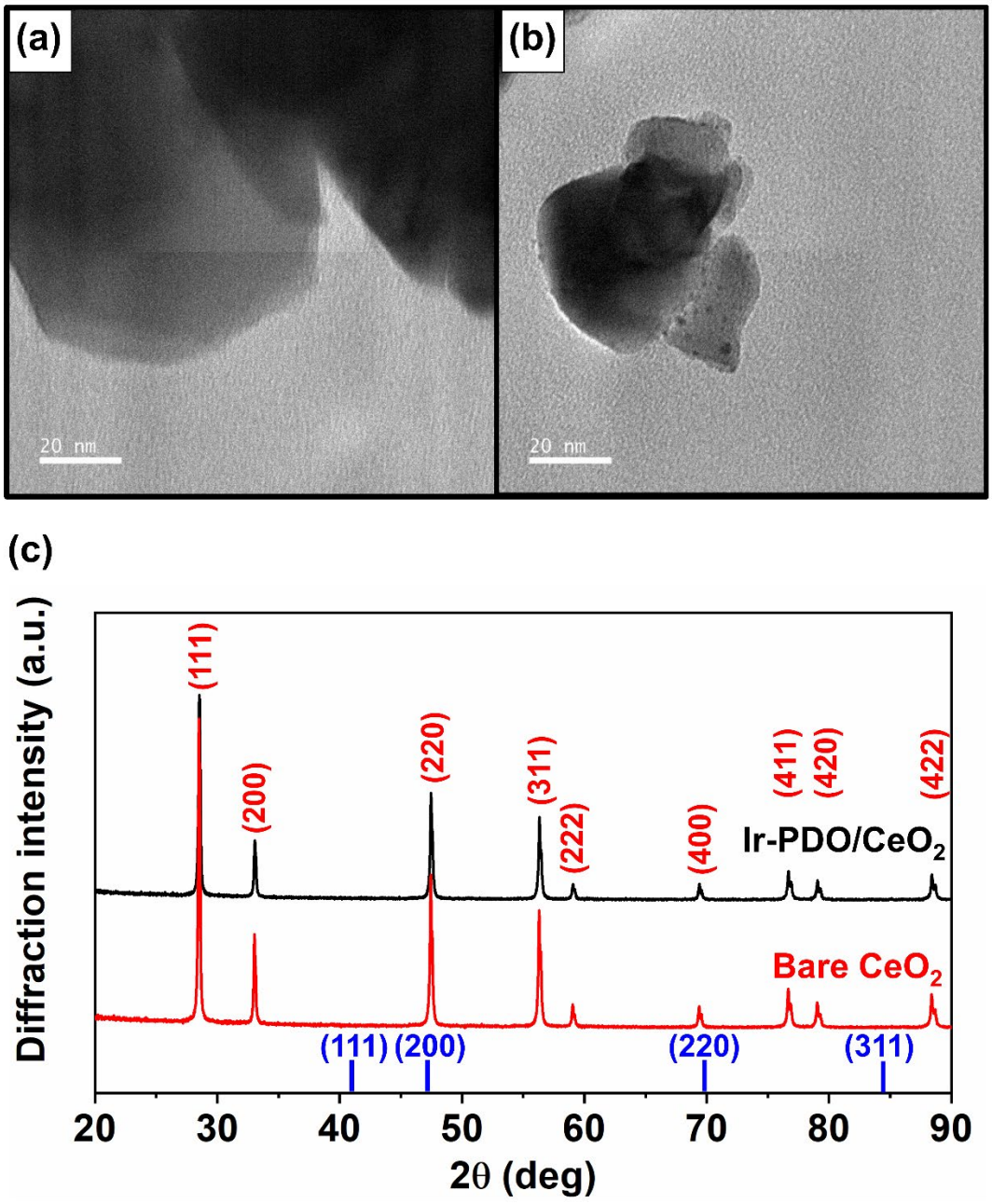

Figure S6. Supplemental characterization results on Ir-PDO/CeO_2. (a) TEM image, showing no visible Ir NPs. (b) TEM image of reduced Ir/CeO_2, showing the appearance of Ir NPs (small blac dots) if present on CeO_2 as a reference. (c) XRD patterns of Ir-PDO/CeO_2 (black) showing only features from CeO_2, identical with bare CeO_2 (red). Peaks from Ir (blue) at theoretical positions are all absent, indicating the absence of crystallized Ir.

Section 3. Supplemental Data Showing Structural Sensitivity

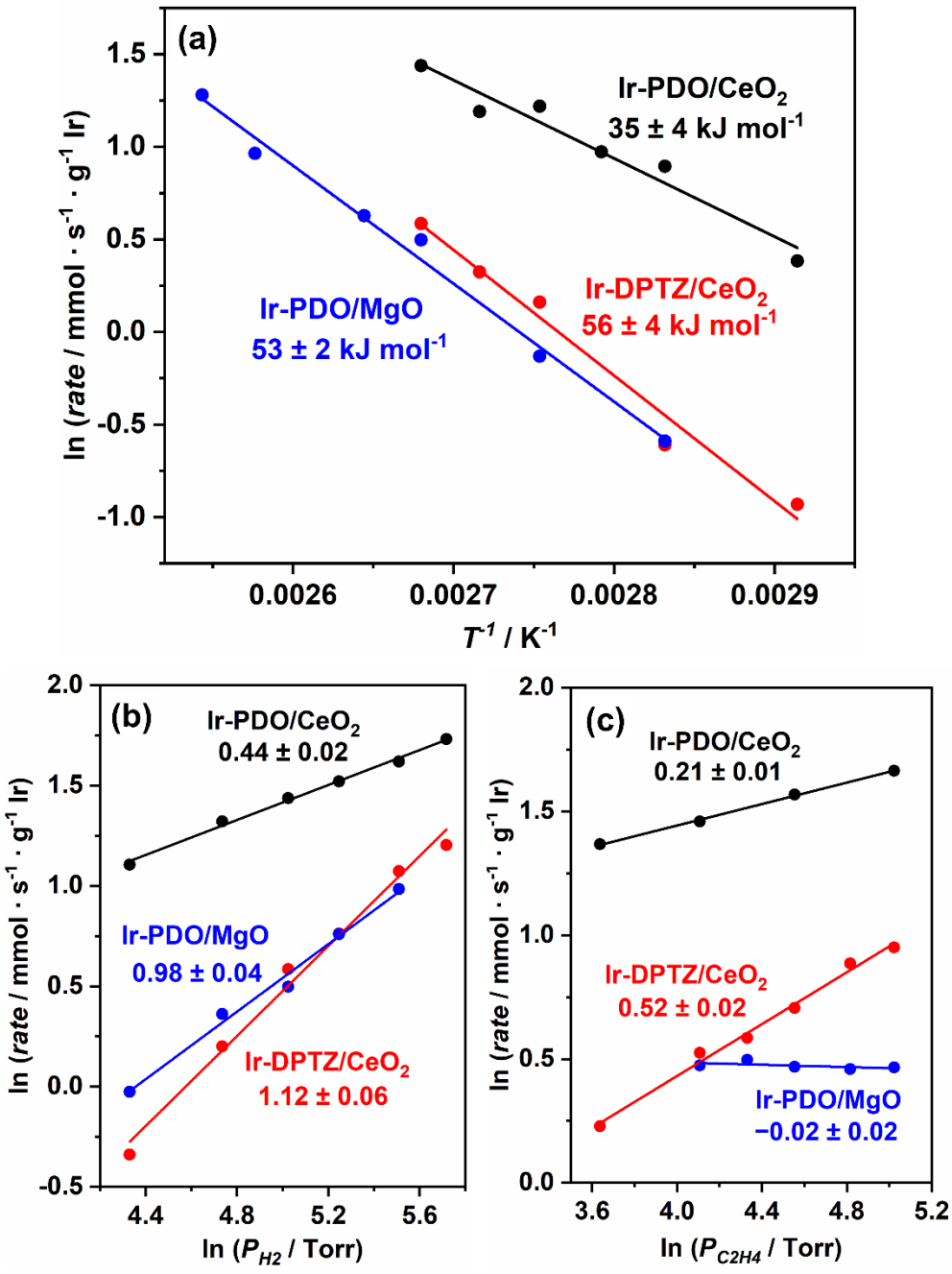

Figure S7. Fittings plots to calculate kinetic parameters in Table 3: (a) apparent activation energy E_a, (b) reaction order with respect to H_2, and (c) reaction order with respect to C_2H_4.

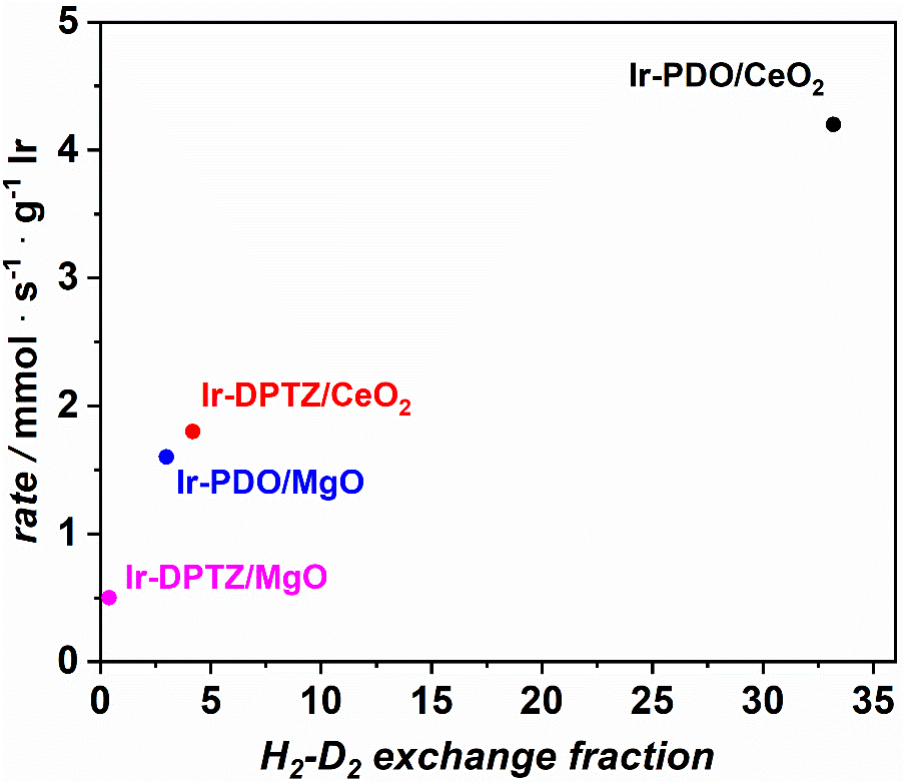

Figure S8. The relationship between the ethylene hydrogenation rate and the H_2-D_2 exchange fraction on four Ir-ligand SACs, showing strong possitive correlation between the two.

Section 4. Supplemental Data for Ir Evolution during H_2/D_2 Exchange Experiments

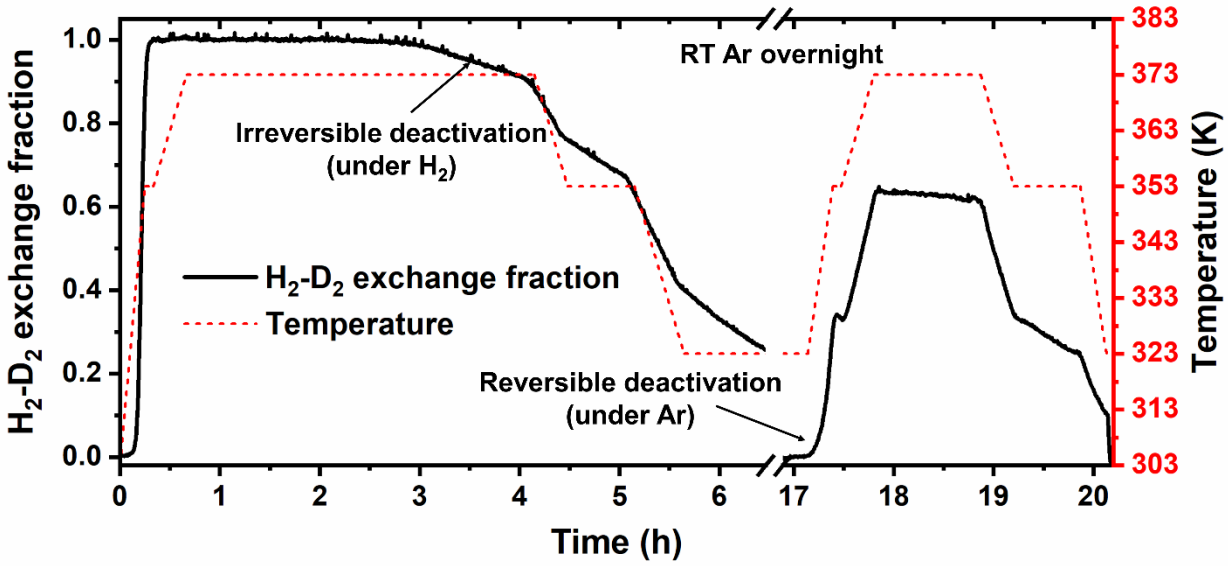

Figure S9. Variations in the H_2-D_2 exchange fraction (relative with equilibrium) over Ir-PDO/MgO SAC with time showing an example of two deactivation pathways under H_2/D_2 and Ar respectively. The black curve and left axis represent the H_2-D_2 exchange fraction, while the red curve and right axis represent temeprature of the catalyst bed. The break on the time axis represents an overnight exposure to pure Ar flow at room temperature.

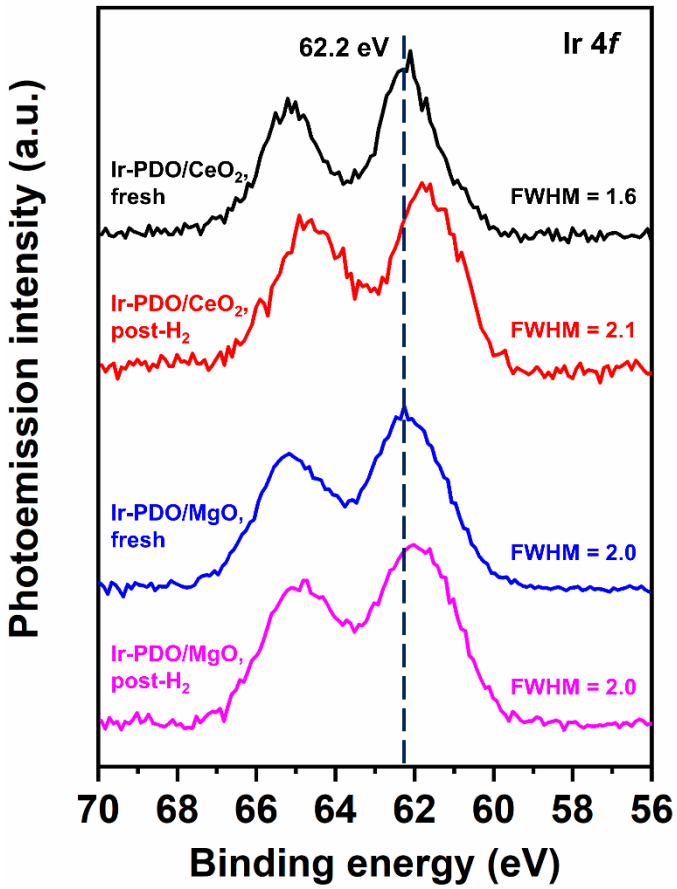

Figure S10. XP spectra of Ir-PDO/CeO_2 and Ir-PDO/MgO SACs after long-term H_2 treatment (red and purple curves respectively) to compare with those of fresh catalysts (black and blue ones respectively), showing signs of slight reduction but not to metallic Ir.

References

1. B. Ravel and M. Newville, *J. Synch. Rad.*, 2005, **12**, 537-541.
2. L. Chen, I. S. Ali, G. E. Sterbinsky, J. T. L. Gamler, S. E. Skrabalak and S. L. Tait, *ChemCatChem*, 2019, **11**, 2843-2854.
3. L. X. Chen, G. E. Sterbinsky and S. L. Tait, *J. Catal.*, 2018, **365**, 303-312.
4. C. Abbehausen, R. E. F. de Paiva, R. Bjornsson, S. Q. Gomes, Z. Du, P. P. Corbi, F. A. Lima and N. Farrell, *Inorg. Chem.*, 2018, **57**, 218-230.
5. Y. Lei, J. Jelic, L. C. Nitsche, R. Meyer and J. Miller, *Top. Catal.*, 2011, **54**, 334-348.
6. S.-Y. Chang, A. Uehara, S. G. Booth, K. Ignatyev, J. F. W. Mosselmans, R. A. W. Dryfe and S. L. M. Schroeder, *RSC Adv.*, 2015, **5**, 6912-6918.
7. B. Sheludko, M. T. Cunningham, A. S. Goldman and F. E. Celik, *ACS Catal.*, 2018, **8**, 7828-7841.